SAND2000-8496C

A Numerical and Experimental Investigation of Premixed Methane-Air Flame Transient Response

Habib N. Najm, Phillip H. Paul, Omar M. Knio†, and Andrew McIlroy
Sandia National Laboratories, Livermore, CA 94550
†The Johns Hopkins University, Baltimore, MD 21218-2686

Corresponding Author: Habib Najm
Sandia National Laboratories
7011 East Ave, MS9051
Livermore, CA 94550
Phone: (925) 294-2054
Fax: (925) 294-2595
Email: hnnajm@ca.sandia.gov

Submitted for oral presentation in Colloquium on Laminar Flames
to the 28^{th} International Symposium on Combustion

Word Count: 3430 (text) + 350 (Refs) + 1800 (figures) = 5580 (total)

Method: unix word count

DISCLAIMER

DISCLAIMER

Portions of this document may be illegible in electronic image products. Images are produced from the best available original document.

Abstract

We report the results of a numerical and experimental investigation of the response of premixed methane-air flames to transient strain-rate disturbances induced by a two-dimensional counter-rotating vortex-pair. The numerical and experimental time histories of flow and flame evolution are matched over a 10 ms interaction time. Measurements and computations of CH and OH peak data evolution are reported, and found to indicate misprediction of the flame time scales in the numerical model. Qualitative transient features of OH at rich conditions are not predicted in the computations. On the other hand, evolution of computed and measured normalized HCO fractions are in agreement. The computed CH_3O response exhibits a strong transient driven by changes to internal flame structure, namely temperature profile steepening, induced by the flow field. Steady state experimental PLIF CH_3O data is reported, but experimental transient CH_3O data is not available. The present analysis indicates that the flame responds at time scales that are quite distinct from "propagation" time scale derived from flame thickness and burning speed. Evidently, these propagation time scales are not adequate for characterizing the transient flame response.

Introduction

The formulation of accurate predictive models of combustion systems requires adequate understanding of turbulence-chemistry interactions at the small scales. One important element of this interaction is the transient response of flames to unsteady perturbations due to turbulent flow structures. The present work uses numerical and experimental studies of the interaction of premixed methane-air flames with two-dimensional counter-rotating vortex pairs to investigate transient flame response and examine comparisons between numerical and experimental results.

There have been both experimental [1-6] and numerical [7-14] studies of flame interaction with counter-rotating vortex pairs or torroidal vortex rings. Experimental studies examined the role of the vorticity field which contorts and strains the flame, and alters its internal structure. These structural changes were observed using Planar Laser-Induced Fluorescence (PLIF) imaging of OH, CH, HCO, CH_2O, and other flame radicals. Early 2D numerical studies of vortex/vortex-pair interactions with premixed flames [7-9] were generally concerned with single-step kinetics, flow dynamics, and thermal effects, rather than internal flame chemical transients. Recent studies [10,11] included C_1 kinetics at stoichiometric conditions to investigate the effect of the vortical flow on internal flame structure.

The use of stiff C_1C_2 mechanisms, which are necessary for accurate prediction of internal flame structure–especially at rich conditions, presents significant additional computational difficulties associated with stiffness and increased complexity due to the large number of species and reactions. These complications are a concern for both explicit and implicit numerical schemes, since the sizes of implicit-scheme matrices and convergence difficulties are accentuated by stiff C_1C_2 kinetics. Najm *et al.* [12] used a detailed C_1C_2 mechanism (GRImech1.2 [15]) to study flame response to unsteady strain-rate and curvature under stoichiometric and rich conditions. However, these studies were limited to a short time span, and fast flow time scales, due to computational costs. These limitations precluded direct comparisons with available experimental results.

The present effort builds on recent numerical developments involving second-order accurate stiff operator-split time integration in multiple dimensions [16,17] to allow detailed resolved computations of stiff 2D C_1C_2 flames at laboratory time scales; a hitherto imprac-

tical undertaking. This removes a barrier to quantitative comparisons with experiments in earlier work, and brings us a step closer to resolving key differences with experimental data.

We use a flow with vortex-strength similar to that in the experiment so that evolution of the flame topology in the two sets of data coincides over a time span of 10 ms. Similarly, we utilize numerical flame stoichiometries and dilution comparable to those in the experiment. We present superimposed transient time histories of computed and experimental flame radicals, and discuss comparisons between them. Despite the matching of operating conditions and the extent of detail in chemistry and transport, we find that the transient flame time scales in the computations are in fact significantly different from those in the experiment. These and other comparisons with the experimental data involving numerical and experimental transient OH, CH, and HCO results are presented and discussed. We also investigate features of the computed transient accumulation of methoxy (CH_3O) and other species on the reactants-side of the flame and analyze the role of unsteady strain-rate in these internal flame dynamics. While no experimental data on the transient response of methoxy in this flame is available, it is hoped that these observations would motivate future measurements to examine their validity.

Model Formulation and Numerical Scheme

The model formulation is presented in detail in [16,17]. The governing equations are developed in 2D using the low Mach number approximation [18] in an open domain. We use a detailed C_1C_2 chemical mechanism. We neglect body forces, Soret and Dufour effects and radiant heat transfer. We assume that the mixture has zero bulk viscosity and that it obeys the equation of state for a perfect gas, with individual species molecular weights, specific heats, and enthalpies of formation. N_2 is assumed dominant such that the diffusion of any other species in the mixture is approximated by binary diffusion into N_2 at the local temperature. For computational efficiency, mixture transport properties are also set to those of N_2 at the local temperature. The chemical production rate for each species is obtained by summing the contributions of Arrhenius-rate elementary reactions, including forward and backward rates and third-body efficiencies [19].

The governing equations are solved using an operator-split stiff second-order predictor-corrector finite difference projection scheme. *Construction of the stiff scheme is based* on several refinements of the explicit construction originally introduced in [10]. A semi-implicit additive (non-split) stiff version is presented in [16]. The present work uses a stiff symmetrically-split integration of the governing equations. Diffusion and convection terms are integrated explicitly with multiple fractional steps, over half-time-step intervals, while the reaction terms are integrated implicitly over a full time-step interval. The explicit half-steps are arranged symmetrically before and after the implicit step in each global step. Stiff integration of reaction terms is performed using DVODE [20].

Experimental Setup and Diagnostics

The experiment has been described in detail in [4,6]. A V-flame is stabilized on a wire in a vertical channel, with premixed methane-air flowing up through flow straighteners upstream of the wire. Line-vortex pairs are ejected from an acoustically driven cavity on one side of the flow enclosure and allowed to impinge on one leg of the V-flame. PLIF imaging of CH, OH and HCO was performed using a XeCl excimer-pumped dye laser and an intensified CCD array detector. For CH the laser was run on a BBQ dye and tuned to the $Q_1(4.5)$ transition of the B-X (0,0) system near 389.5 nm, with non-resonant detection using 2 mm of Schott GG-420 and an F/1.2 camera lens. For OH the laser was run on a C153 dye, doubled in BBO and tuned to the $Q_1(6.5)$ A-X (1,0) transition near 283 nm, with non-resonant detection using 2 mm of Schott WG305 and an F/4.5 UV camera lens. For HCO, the laser was run on a C500 laser dye, doubled in BBO and tuned to ${}^{Q}R_0$ bandhead in the B-X (0,0,0) system near 254 nm, with non-resonant detection using 2 mm of Schott BG1, a 400 nm reflective short-pass and an F/2.2 transmissive UV lens system.

PLIF images of CH_3O have also been successfully taken in the same burner, using the same laser/camera system but under steady conditions. The laser was operated as for pumping OH and tuned to excite overlapping transitions in the A-X 3_0^4 system near 292.8 nm with care taken to avoid excitation of adjacent OH and CH_2O transitions. Non-resonant detection was performed using 2 mm of Schott WG320, a 400 nm reflective short-pass filter and an F/1.4 near-UV camera lens. As found with PLIF of HCO [11], CH_3O PLIF signals are quite weak and frame averaging is required to achieve a useable image (nominally 50-frame averages are required for imaging in a premixed 30% N_2-diluted stoichiometric CH_4-air flame).

Results

In both the experiments and computations, two CH_4-air reactants mixture conditions are investigated: one stoichiometric and the other rich, with equivalence ratio $\Phi = 1.2$. Both numerical flames use 32% N_2-diluted reactants, thus justifying the above assumed dominance of N_2 in the transport model. The experimental rich flame uses this same dilution, while the stoichiometric flame dilution is slightly higher, at 36%.

Flow-Flame Evolution

An open rectangular domain is considered, with dimensions 0.4×1.6 cm, and is overlaid by a 256×1024 uniform mesh. We apply symmetry boundary conditions in the horizontal x-direction, and outflow boundary conditions in the y-direction. The evolution of the flow over a 12 ms time span is illustrated in Figure 1 for the stoichiometric flame. The evolution of the rich flame is similar. The vertical right edge of the domain is the centerline of the vortex pair under consideration, which is one member of a periodic row of vortex pairs along the x-direction. The initial condition is a superposition of the velocity (u,v) field induced by the periodic row of vortex pairs, and the temperature, density and mass fraction (T,ρ,Y_i) distributions corresponding to a horizontal premixed flame, with the initial structure in the y-direction from a 1D flame solution computed with Chemkin [19,21]. We use a C_1C_2 chemical mechanism with 40 species and 216 reactions. It is based on a subset of the mechanism used in [22], and is available upon request.

The flame propagates downward by burning into the reactants, as shown in Figure 1. Meanwhile, the vortex pair propagates upwards causing transient curvature and strain-rate disturbances to the flame. A typical experimental CH frame sequence, which exhibits comparable flame topology evolution with time as in Fig. 1, is reported in [4]. The time reference in the subsequent comparisons between experimental and numerical results is determined based on matching flame topology in the set of frames in the sequence shown in the Figure.

The initial center-to-center distance (δ_{cc}) of the vortex pair is 0.25 cm, and its self-induced propagation speed ranges from 30 cm/sec at $t = 0$ to 110 cm/sec at 10 ms. The experimental vortex-pair self-induced velocity is also found to increase in time, ranging from 100 to 150 cm/sec during the interaction. The experimental vortex-pair center-to-center

distance is about 0.4 cm, and the diameter of the flame bubble (e.g. 8 ms frame in Fig. 1) is about 0.8 cm. Thus, the numerical flame bubble is about 1/2 that of the experimental one.

Based on the numerical vortex-pair mean $\delta_{cc} = 0.21$ cm, its mean self-induced velocity $V_v = 62$ cm/s, and the associated experimental vortex-pair $\delta_{cc} = 0.4$ cm and $V_v = 125$ cm/s, the convective time scales of the numerical and experimental vortex pairs are roughly the same, at $t_v \approx 3.2$ ms. Using time scales based on flame thermal thickness and burning speed, the two flames considered here ($\Phi = 1.0$ and 1.2) have time scales $t_f = 13.5$ and 49.1 ms respectively. On the other hand, as reported in [12] and further discussed below, these propagation time scales are very different from those exhibited by the flame response to the unsteady strain.

OH *and* CH *Response*

The evolution of normalized peak rich flame quantities from the numerical and experimental results are shown on the same time axis in Figure 2. The overall numerical flame response is seen to exhibit slow decay over a time interval of 6-7 ms. A roughly 50% drop in heat release rate w_T is evident, along with coincident decay profiles of HCO and OH. CH exhibits similarly slow decay, down to about 30% of its original level. The experimental flame on the other hand exhibits drastically different behavior. There is practically no drop in either OH or CH signals over the first 5 ms of flame evolution. This is then followed by simultaneous and opposite fast response of both signals. OH increases by a factor of 3.5 in 1 ms, and then decays over the remaining 4 ms. On the other hand, CH signal drops quickly, reaching zero in 2 ms, and disappearing thereafter. Given the similar flow and flame time scales in the numerical and experimental flows, these disagreements in qualitative response (of OH) and transient time scales (of both OH and CH) are remarkable.

The evolution of the stoichiometric flame peak quantities are shown in Figure 3. In this case, the experimental and numerical flames exhibit qualitatively similar monotonically decaying behavior in both OH and CH, yet with significant quantitative disagreement. Let us first compare this data with that of the rich case in Fig. 2. There is more decay of the numerical peak quantities in the weaker rich flame. On the other hand, the experimental CH data shows similar decay to zero in both cases, albeit with faster decay rate in the rich case as indicated in [12]. Moreover, the burst in OH observed at rich conditions is absent

from the experimental stoichiometric data, with monotonic decay of OH observed down to 60% of the initial undisturbed flame value. Next, compare the experimental and numerical stoichiometric flame results. As in the rich case, experimental signals of peak OH and CH exhibit faster time scales and higher degrees of change in amplitude than the corresponding numerical signals.

At present, an explanation for the burst in experimental OH at rich conditions is lacking. It is also not clear if the absence of this burst from the computational results is due to missing reaction pathways or inaccuracies in species transport properties [23] and/or reaction rate parameters. Note, however, that the accumulation of species during flame transients is not surprising since different reaction pathways have different characteristic time scales which generally depend on mixture stoichiometry [12]. Such transient accumulations are in fact observed in the computations, as further discussed below.

HCO *Response*

Figure 3 also shows experimental peak HCO data over a 4 ms time span. The HCO data has low signal to noise ratio, with 10% uncertainty. Still, it is interesting to note that the relative evolution of this signal does not deviate much from the numerical HCO and heat release data. No experimental HCO data is available later on in the cycle, which limits the scope of the comparison. Nevertheless, the agreement up to 6 ms is encouraging (even as the experimental CH deviates strongly downward) and suggests that the present mechanism may be reasonably capturing at least some components of transient flame structure.

In earlier work [11,24] we noted the fidelity with which peak numerical HCO mole fraction correlates with peak flame heat release rate of premixed methane-air flames. This observation is borne out in the present results as well. Computed peak HCO mole fraction provides a reasonably good representation of peak heat release rate in both Figs. 2 and 3, better than computed OH or CH.

Moreover, if we accept the correspondence between HCO and heat release rate, then the robustness of the experimental HCO signal at 6 ms in Fig. 3 suggests that the stoichiometric flame is in fact able to withstand the present rate of strain without extinction. This is despite the strong drop in CH signal evident in the figure. The drop in CH is of course indicative of significant disruption of flame chemistry in certain portions of the chemical mechanism.

However, since the bulk of the carbon flux is through HCO and not through CH [11], these disruptions are not necessarily indicative of overall extinction of the flame.

CH_3O *Response*

In the present mechanism, the methoxy radical (CH_3O) is produced primarily by the reaction $CH_3+HO_2 \rightarrow CH_3O+OH$, and consumed by $CH_3O(+M) \rightarrow CH_2O+H(+M)$. The mole fraction profile of methoxy in the undisturbed rich flame is shown in Fig. 4 ($t = 0$). We focus on the rich flame data because it exhibits more significant changes in time, though it is qualitatively similar to that in the stoichiometric flame. The $t = 0$ profile in Fig. 4 reveals two distinct peaks of CH_3O. The one nearer to the zero abscissa is within the fuel consumption zone. Peak fuel consumption rate occurs at $x = 0.014$ and drops below 5% of peak at $x = -0.05$. The outer peak at $x = -0.11$ exists in a low temperature region (see Fig. 6). The methoxy profile in Fig. 4 shows opposite evolution of the two peaks. The high temperature peak decays in time, in accordance with decaying peak burning and heat release rates; while the low temperature peak exhibits a rising transient, increasing by a factor of 3 in the first 3 ms of the interaction, followed by a gradual decay, viz. the 8 ms profile. Strain-rate and temperature fields during this process, shown in Figs. 5 and 6 respectively, suggest the essential causes of this transient. The strain-rate rises in time in the flame reference frame, peaking at 3-4 ms, and then decays. Meanwhile, the temperature profile steepens due to the rising strain-rate, as shown in Fig. 6, leading to lower temperatures in the region with $T < 1000$ K. By $t \sim 8$ ms this steepening subsides and, despite the reduced burning rate, the temperature on the reactant side increases due to the inundation of the reaction zone with hot combustion products [10].

Despite the observed opposite trends in CH_3O mole fraction in the two peaks in Fig. 4, we note that its dominant production and consumption channels both decay during the process, as shown in Fig. 7. On the other hand, the net production rate of methoxy clearly exhibits a fast rising transient in the low temperature region, as shown in Fig. 8, which leads to the observed transient accumulation in Fig. 4. In contrast, and consistent with the behavior of the high temperature peak in Fig. 4, both production and consumption rates in the high temperature region in Fig. 8 decay in time. Analysis of the results indicates that the net increase in production rate of CH_3O on the cold side of the flame is driven primarily

by the local temperature drop in Fig. 6. Reaction 51 (CH_2O+H(+M)=CH_3O(+M)) has a high activation barrier in the reverse direction, such that a drop in temperature leads to a reduction in the reverse (consumption) rate. Despite opposing factors, a large net increase in the production rate of CH_3O occurs, as seen in Fig. 8. Note that the balance of Reactions 51 and 32 (Fig. 7) in the high temperature region would have lead to a similar increase of CH_3O production rate there, were it not for the decay of the reaction CH_3OH+H=CH_3O+H_2, a production channel, due to reduced H.

We do not have transient measurements of methoxy to validate the above findings. However, PLIF data on methoxy in the steady V-flame is available; it is compared to the initial data from the computations. These experimental profiles of CH_3O PLIF signal, taken across the primary flame, show a single well-defined peak co-located with the reactant-side inflection point in the experimental CH_2O profiles [6]. This is in contrast to the computed profiles in Fig. 4, which show a double-peaked structure. PLIF signal is proportional to the mole fraction of the target species and to a complex function of temperature and composition of the collisional bath. For CH, OH and HCO, which exist in a relatively limited range of conditions, transitions can be selected in the experiment to minimize these residual dependencies. CH_3O, however, has four strong vibrational modes active under flame conditions [25], leading to a strong decrease in signal with temperature. Thus the absence of a double-peaked profile in the experimental data may be the result of the temperature dependence in the CH_3O signal. Alternatively, it is possible that small changes in the temperature dependence in reactions 51 and 32 could result in a single CH_3O peak in the computations.

Conclusions

We have presented time-matched numerical and experimental results describing the detailed interaction of a premixed methane-air flame with a counter-rotating vortex pair in 2D.

We observe a transient rise in computed methoxy (CH_3O) on the cold side of the flame during the interaction. We attribute this to changes in internal flame structure caused by the transient flow-induced strain-rate. In particular, the flow-induced steepening of the temperature profile lowers the temperature on the reactants side of the reaction zone, leading to reduced consumption of CH_3O. We have also observed this transient behavior of methoxy using the GRImech1.2 mechanism, and at other degrees of N_2-dilution, as well as other flow time scales. Generally, the extent of the rise in peak CH_3O is higher with the less robust flames and with the faster flows. We also find similar transient accumulation in two other species on the cold side of the flame, namely CH_3O_2 and C_2H_2OH, with similar–although milder–behavior in CH_3CO. We discuss experimental measurements of CH_3O in a steady V-flame, which outline potential difficulties with PLIF of CH_3O at high temperature. Measurements of CH_3O during the flame interaction with the vortex-pair are necessary to validate the above observed transients.

We report experimental measurements of peak HCO evolution, that are in reasonable agreement with numerical results, suggesting continued burning despite the collapse of the CH signal.

We find significantly faster response of CH and OH in the experiment, versus the computed CH and OH under both stoichiometric and rich conditions. We also observe qualitatively different response of OH at rich conditions. These findings suggest that the present diffusion-reaction model does a poor job at the representation of the dynamical character of OH and CH in this flame. Assignment of the causes of these disagreements requires analysis of the coupled reaction-diffusion eigenmodes of the governing equations, which is work in progress.

The qualitative disagreement in rich-flame OH response was observed earlier [12] using GRImech1.2 [15] with ten-fold faster flow time scales, and is found here with flow time scales comparable to the experiment, using an alternate C_1C_2 chemical mechanism. These observations, and the above general disagreement in computed and measured flame time scales

of OH and CH, indicate the extent to which validation of detailed unsteady flame models is lacking. This is true whether the cause of these disagreements is transport coefficients or the chemical mechanism. Clearly, validation under steady state conditions is insufficient. The dynamical response of the model requires experimental and computational studies that probe the transient structure of flames. Additional work along these lines is necessary to provide clues as to the causes of these disagreements, and to examine the relative merits of alternative mechanisms or transport models.

Acknowledgments

This work was supported by the US Department of Energy, Office of Basic Energy Sciences, Chemical Sciences Division.

References

[1] Roberts, W.L., Driscoll, J.F., Drake, M.C., and Goss, L.P., *Combustion and Flame*, 94:58–69 (1993).

[2] Samaniego, J.-M., Annual research briefs, Center for Turbulence Research, Stanford University/NASA Ames Research Center, (1993).

[3] Mueller, C.J., Driscoll, J.F., Sutkus, D.J., Roberts, W.L., Drake, M.C., and Smooke, M.D., *Combustion and Flame*, 100:323–331 (1995).

[4] Nguyen, Q.-V., and Paul, P.H., *Twenty-Sixth Symposium (International) on Combustion*, The Combustion Institute, pp. 357–364, (1996).

[5] Mueller, C.J., Driscoll, J.F., Reuss, D.L., Drake, M.C., and Rosalik, M.E., *Combustion and Flame*, 112(3):342–358 (1998).

[6] Paul, P.H., and Najm, H.N., *Twenty-Seventh Symposium (International) on Combustion*, The Combustion Institute, pp. 43–50, (1998).

[7] Ashurst, W.T., and McMurtry, P.A., *Comb. Sci. Tech.*, 66:17–37 (1989).

[8] Rutland, C.J., and Ferziger, J.H., *Combustion and Flame*, 84:343–360 (1991).

[9] Poinsot, T., Veynante, D., and Candel, S., *J. Fluid Mechanics*, 228:561–606 (1991).

[10] Najm, H.N., and Wyckoff, P.S., *Combustion and Flame*, 110(1-2):92–112 (1997).

[11] Najm, H.N., Paul, P.H., Mueller, C.J., and Wyckoff, P.S., *Combustion and Flame*, 113(3):312–332 (1998).

[12] Najm, H.N., Knio, O.M., Paul, P.H., and Wyckoff, P.S., *Combustion Theory and Modelling*, 3(4):709–726 (1999).

[13] Katta, V.R., Carter, C.D., Fiechtner, G.J., Roquemore, W.M., Gord, J.R., and Rolon, J.C., *Twenty-Seventh Symposium (International) on Combustion*, The Combustion Institute, pp. 587–594, (1998).

[14] Patnaik, G., and Kailasanath, K., *Twenty-Seventh Symposium (International) on Combustion*, The Combustion Institute, pp. 711–717, (1998).

[15] Frenklach, M., Wang, H., Goldenberg, M., Smith, G.P., Golden, D.M., Bowman, C.T., Hanson, R.K., Gardiner, W.C., and Lissianski, V., Top. Rep. GRI-95/0058, GRI, (1995).

[16] Najm, H.N., Wyckoff, P.S., and Knio, O.M., *J. Comp. Phys.*, 143(2):381–402 (1998).

[17] Knio, O.M., Najm, H.N., and Wyckoff, P.S., *J. Comp. Phys.*, 154:428–467 (1999).

[18] Majda, A., and Sethian, J., *Comb. Sci. and Technology*, 42:185–205 (1985).

[19] Kee, R.J., Rupley, F.M., and Miller, J.A., Sandia Report SAND89-8009B, Sandia National Labs., Livermore, CA, (1993).

[20] Brown, P.N., Byrne, G.D., and Hindmarsh, A.C., *SIAM J. Sci. Stat. Comput.*, 10:1038–1051 (1989).

[21] Kee, R.J., Grcar, J.F., Smooke, M.D., and Miller, J.A., Sandia Report SAND85-8240, Sandia National Labs., Livermore, CA, (1993).

[22] Prada, L., and Miller, J.A., *Combust. Sci. and Tech.*, 132:225–250 (1998).

[23] Paul, P., and Warnatz, J., *Twenty-Seventh Symposium (International) on Combustion*, The Combustion Institute, pp. 495–504, (1998).

[24] Najm, H.N., Knio, O.M., Paul, P.H., and Wyckoff, P.S., *Comb. Sci. Tech.*, 140(1-6):369–403 (1998).

[25] Garland, N.L., and Crosley, D.R., *J. Phys. Chem.*, 92:5322–5326 (1988).

Figure Captions

Figure 1. Evolution of CH mole fraction (shading) and vorticity (contours) for the stoichiometric flame.

Figure 2. Evolution of the computed peak heat release rate (w_T) and peak CH, OH, and HCO mole fractions on the rich flame centerline. Experimental data for peak CH and OH are superimposed.

Figure 3. Evolution of the computed peak heat release rate (w_T) and peak CH, OH, and HCO mole fractions on the stoichiometric flame centerline. Experimental data for peak CH, OH, and HCO are superimposed.

Figure 4. Instantaneous computed CH_3O mole fraction profiles along a normal cut at the rich flame centerline. Data is taken in a reference frame moving with the flame, with x-distance measured from the location of the fuel mass fraction contour corresponding to 10% of the reactants fuel mass fraction. Reactants are on the left, and products on the right. Solid lines are for [0-4] ms as indicated, while the dashed line is at 8 ms.

Figure 5. Instantaneous tangential strain-rate profiles along a normal cut at the rich flame centerline. Data is taken in a reference frame moving with the flame as in Fig. 4. Solid lines are for [0-4] ms as indicated, while the dashed line is at 8 ms.

Figure 6. Instantaneous temperature profiles along a normal cut at the rich flame centerline. Data is taken in a reference frame moving with the flame as in Fig. 4. Solid lines are for [0-4] ms as indicated, while the dashed line is at 8 ms.

Figure 7. Instantaneous profiles of the two dominant reaction rates involving CH_3O along a normal cut at the rich flame centerline. Data is taken in a reference frame moving with the flame as in Fig. 4.

Figure 8. Instantaneous profiles of the net production rate of CH_3O along a normal cut at the rich flame centerline. Data is taken in a reference frame moving with the flame as in Fig. 4. Solid lines are for [0-4] ms as indicated, while the dashed line is at 8 ms.

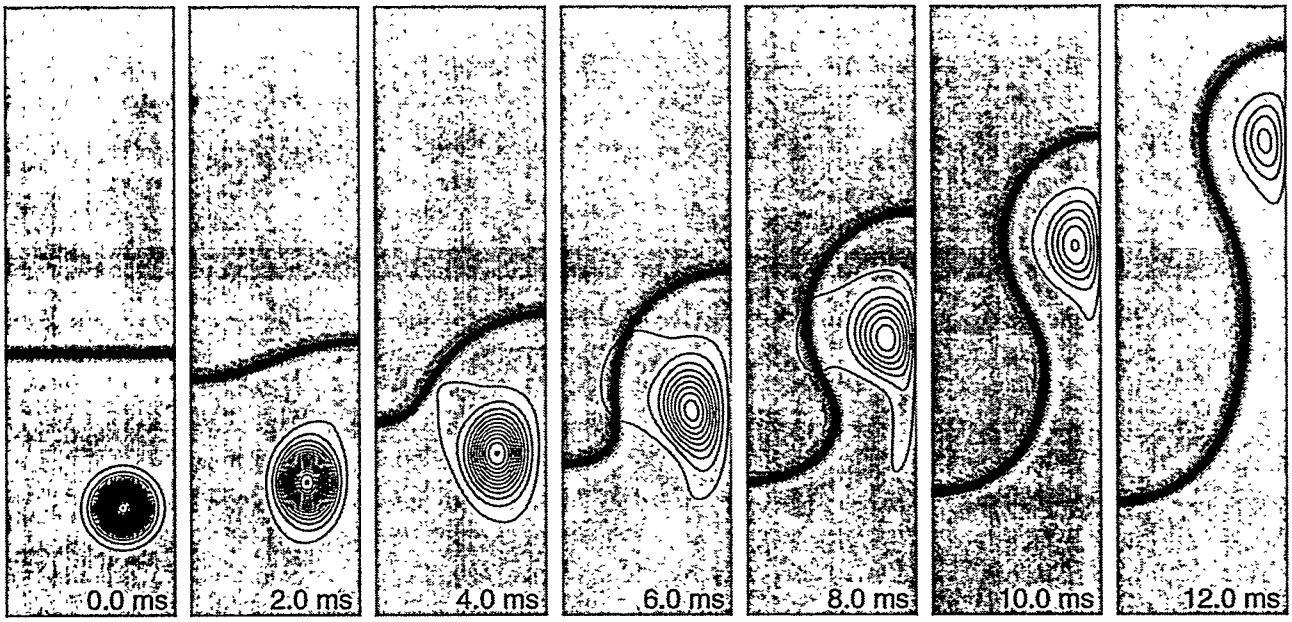

Figure 1. Evolution of CH mole fraction (shading) and vorticity (contours) for the stoichiometric flame.

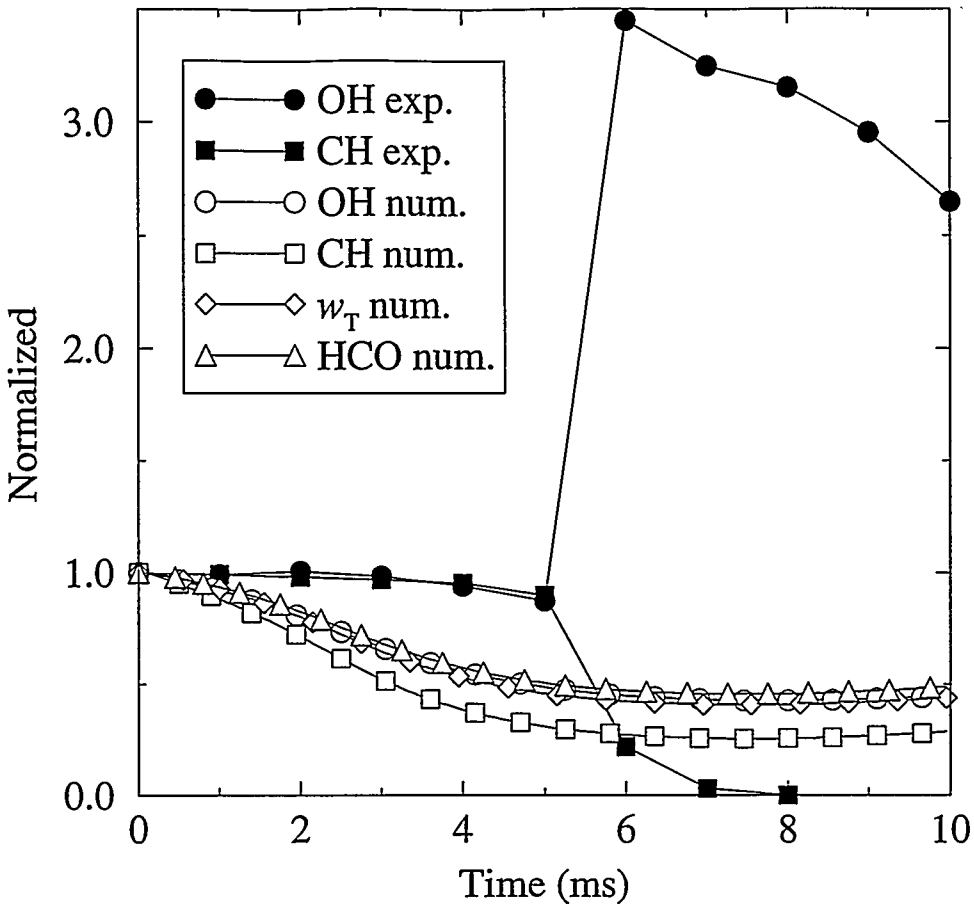

Figure 2. Evolution of the computed peak heat release rate (w_T) and peak CH, OH, and HCO mole fractions on the rich flame centerline. Experimental data for peak CH and OH are superimposed.

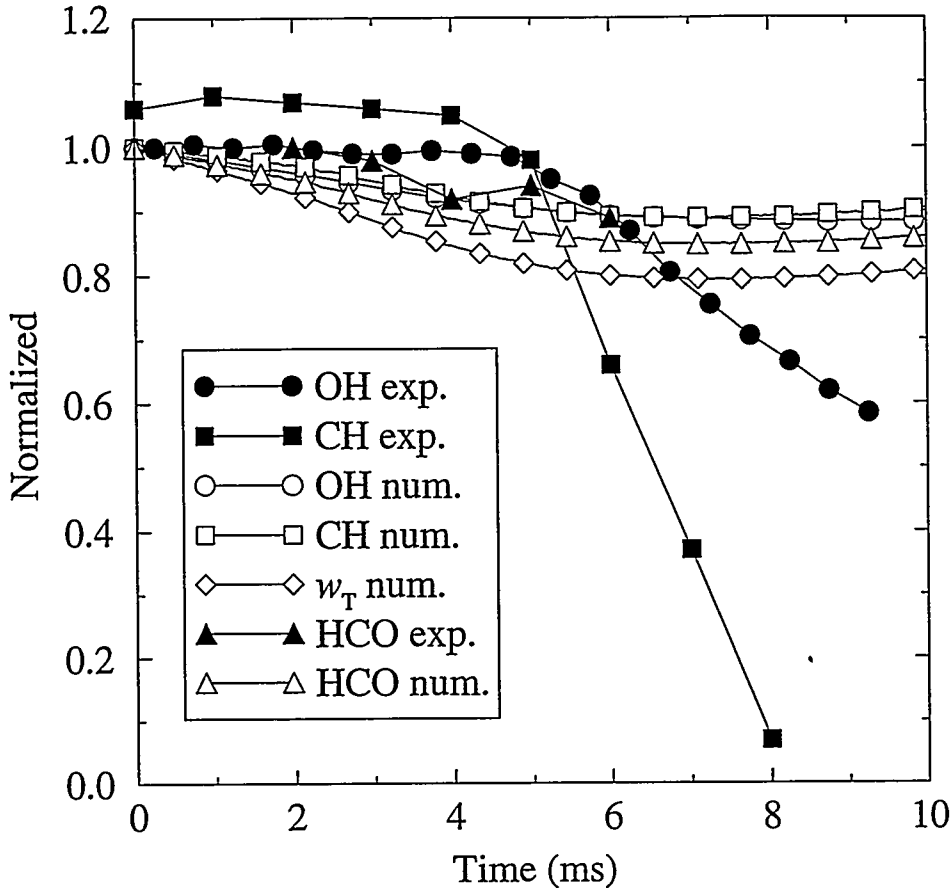

Figure 3. Evolution of the computed peak heat release rate (w_T) and peak CH, OH, and HCO mole fractions on the stoichiometric flame centerline. Experimental data for peak CH, OH, and HCO are superimposed.

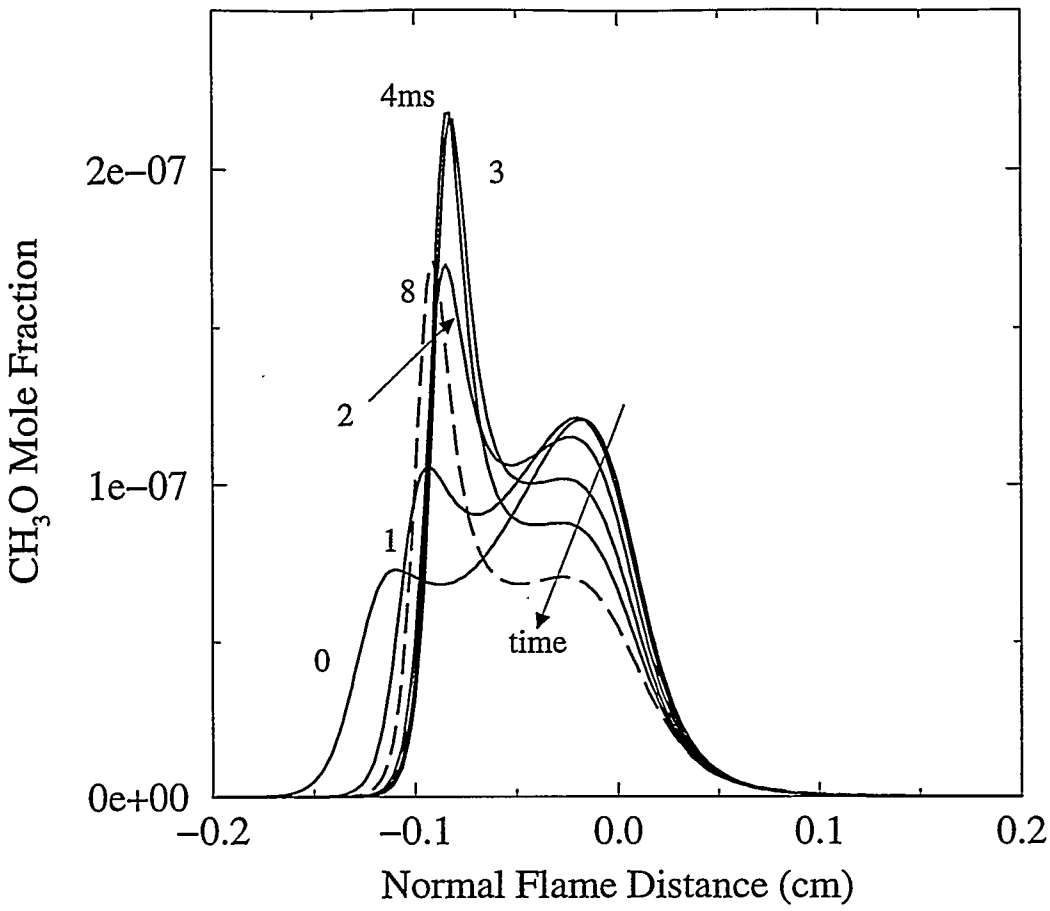

Figure 4. Instantaneous computed CH_3O mole fraction profiles along a normal cut at the rich flame centerline. Data is taken in a reference frame moving with the flame, with x-distance measured from the location of the fuel mass fraction contour corresponding to 10% of the reactants fuel mass fraction. Reactants are on the left, and products on the right. Solid lines are for [0-4] ms as indicated, while the dashed line is at 8 ms.

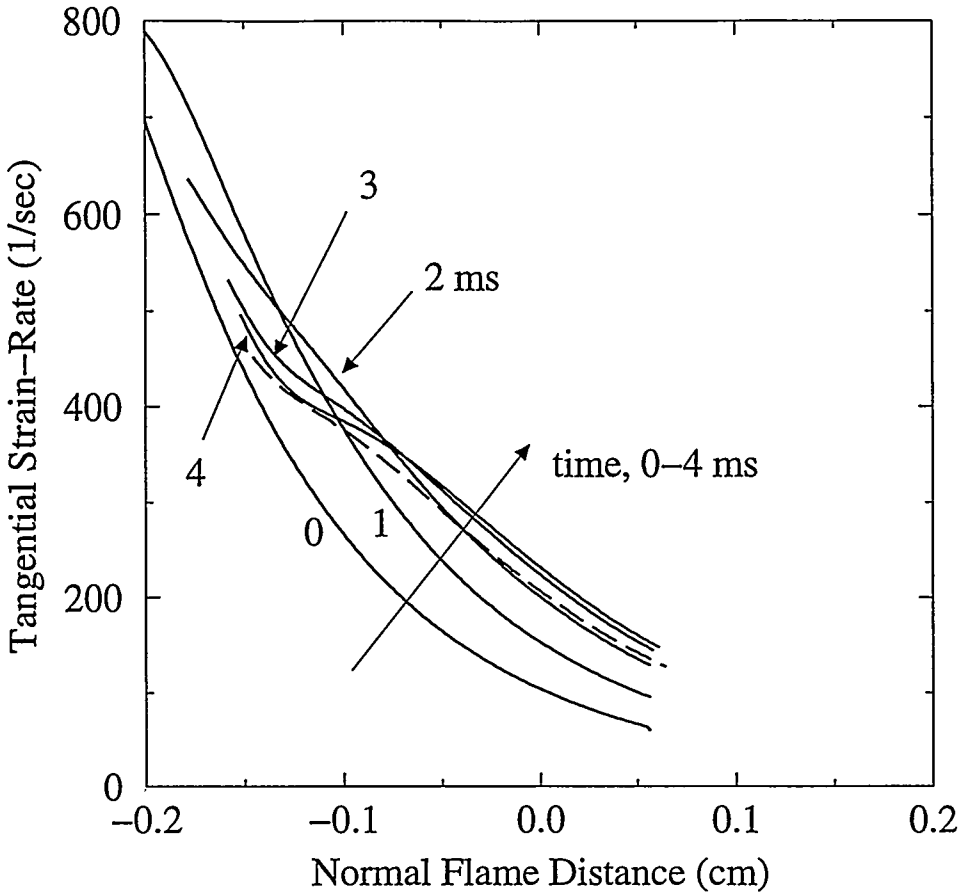

Figure 5. Instantaneous tangential strain-rate profiles along a normal cut at the rich flame centerline. Data is taken in a reference frame moving with the flame as in Fig. 4. Solid lines are for [0-4] ms as indicated, while the dashed line is at 8 ms.

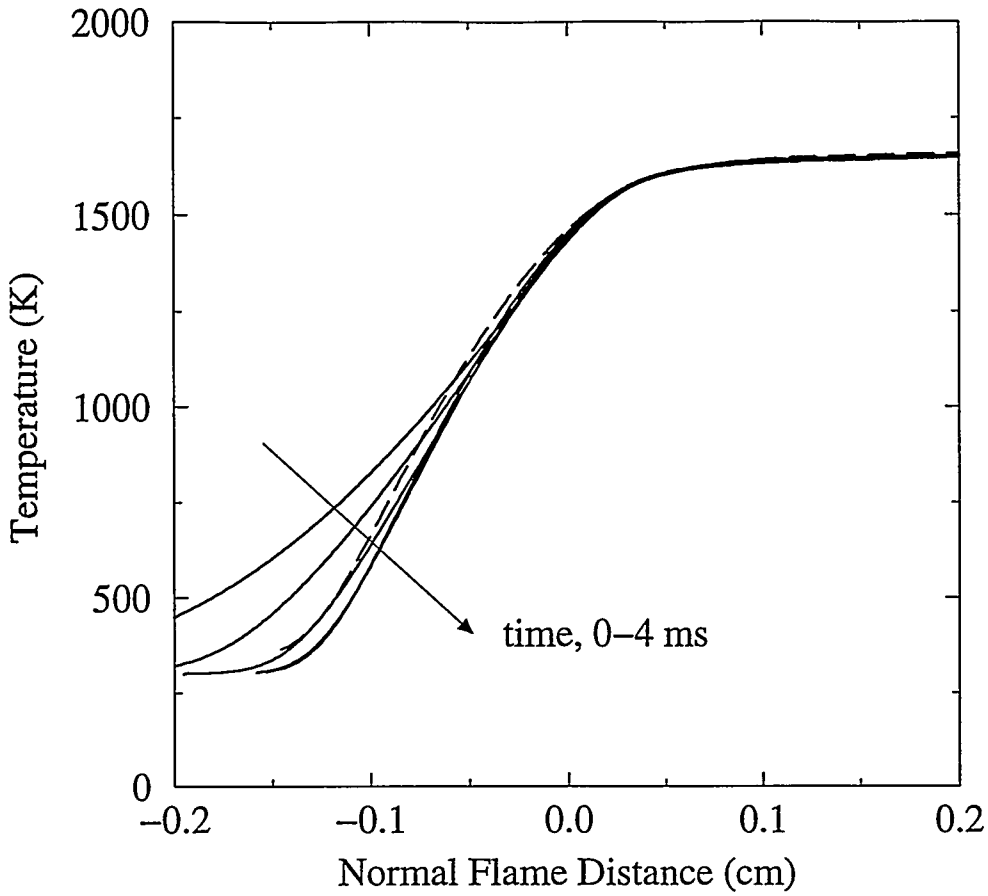

Figure 6. Instantaneous temperature profiles along a normal cut at the rich flame centerline. Data is taken in a reference frame moving with the flame as in Fig. 4. Solid lines are for [0-4] ms as indicated, while the dashed line is at 8 ms.

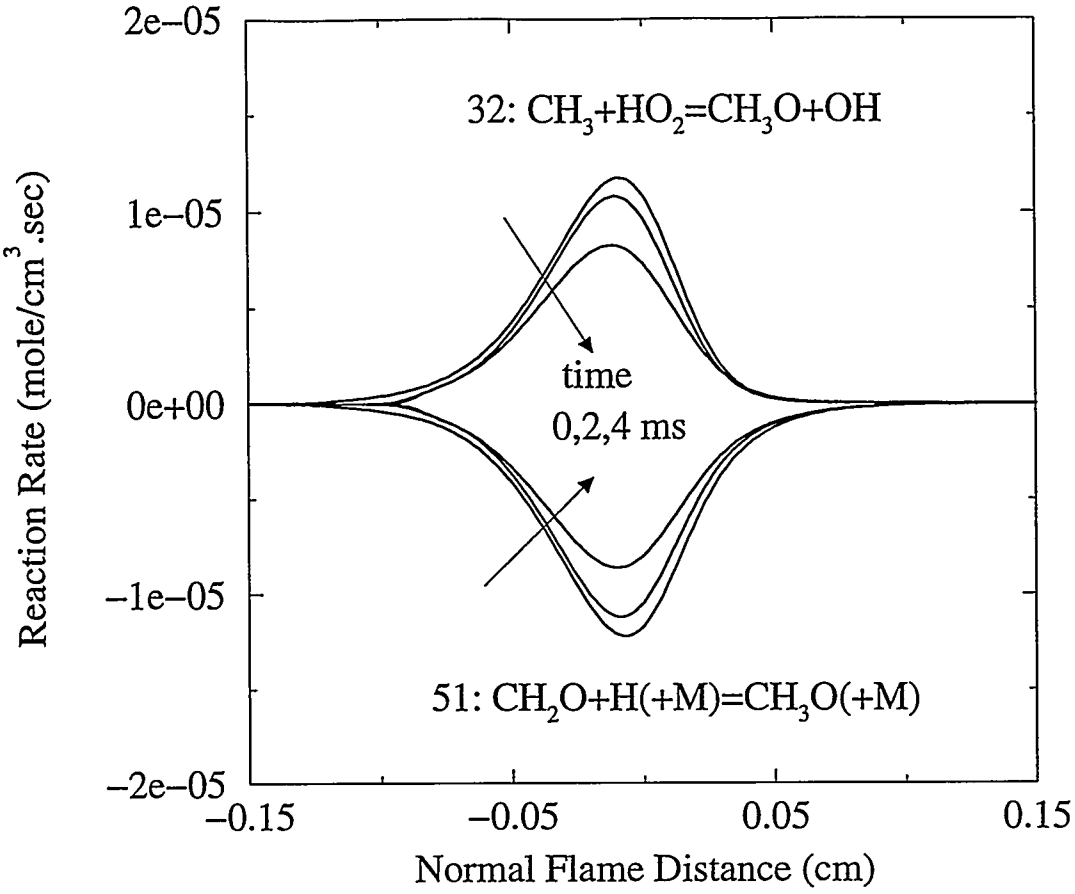

Figure 7. Instantaneous profiles of the two dominant reaction rates involving CH_3O along a normal cut at the rich flame centerline. Data is taken in a reference frame moving with the flame as in Fig. 4.

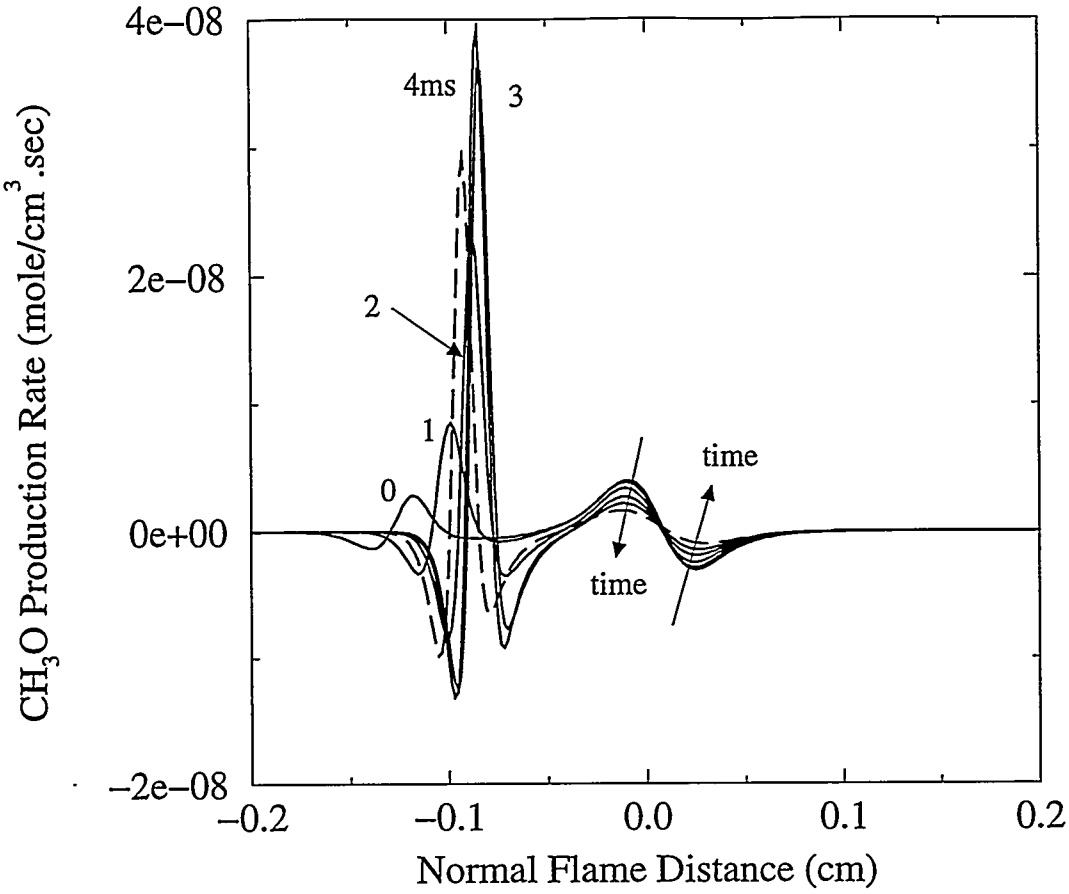

Figure 8. Instantaneous profiles of the net production rate of CH_3O along a normal cut at the rich flame centerline. Data is taken in a reference frame moving with the flame as in Fig. 4. Solid lines are for [0-4] ms as indicated, while the dashed line is at 8 ms.